https://doi.org/10.5194/tc-2020-9
Preprint. Discussion started: 6 February 2020
© Author(s) 2020. CC BY 4.0 License.

The Cryosphere Discussions

The role of electrical conductivity in radar wave reflection

Slawek M. Tulaczyk[1], Neil T. Foley[1]

[1]Department of Earth and Planetary Sciences, University of California, Santa Cruz, CA 95064, USA

Correspondence to: Slawek M. Tulaczyk (stulaczy@ucsc.edu)

Abstract. We have examined a general expression giving the specular reflection coefficient for a radar wave approaching a reflecting interface with normal incidence. The reflecting interface separates two homogeneous isotropic media, the properties of which are fully described by three scalar quantities: dielectric permittivity, magnetic permeability, and electrical conductivity. The derived relationship indicates that electrical conductivity should not be neglected *a priori* in glaciological investigations of subglacial materials, and in GPR studies of saturated sediments and bedrock, even at the high end of typical linear radar frequencies used in such investigations (e.g., 100 MHz). Our own experience in resistivity surveying in Antarctica, combined with a literature review, suggests that a wide range of geologic materials can have electrical conductivity that is high enough to significantly impact the value of radar reflectivity. Furthermore, we have given two examples of prior studies in which inclusion of electrical conductivity in calculation of the radar bed reflectivity may provide an explanation for results that may be considered surprising if the impact of electrical conductivity on radar reflection is neglected. The commonly made assumption that only dielectric permittivity of the two media need to be considered in interpretation of radar reflectivity can lead to erroneous conclusions.

https://doi.org/10.5194/tc-2020-9
Preprint. Discussion started: 6 February 2020
© Author(s) 2020. CC BY 4.0 License.

The Cryosphere Discussions

1 Introduction

Ice penetrating radar represents the most successful geophysical technique in glaciology, that efficiently yields observational constraints on fundamental properties of land ice masses on Earth, such as thickness, internal structures, and bed properties (e.g., reviews in Plewes and Hubbard, 2001; Dowdeswell and Evans, 2004). Radar has also been used to investigate ice masses on Mars (e.g., Holt et al., 2008; Bierson et al., 2016) and will be used to probe ice shells on icy satellites (e.g., Chyba et al., 1998; Aglyamov et al., 2017). Much of the success of radar imaging in glaciology can be attributed to the fact that glacier ice is a polycrystalline solid with either no, or little, liquid water and low concentration of impurities from atmospheric deposition, e.g., sea salts and acidic impurities (Stillman et al., 2013). Hence, glacier ice is a poor electrical conductor and is quite transparent to electromagnetic waves over a broad range of frequencies (Dowdeswell and Evans, 2004).

Electrical conductivity is the material property that controls attenuation of electromagnetic waves (Stratton, 1941) and the resistive nature of glacier ice makes it reasonable to assume that it is a nearly lossless material with regards to radar wave propagation. However, as illustrated by the research on the origin of internal radar reflectors in ice sheets and glaciers, radar reflections can be caused by contrasts in either real permittivity or conductivity, even though such englacial contrasts are quite small for both of these material properties (Paren and Robin, 1975). These authors developed two different equations for the radar reflection coefficient, which express the dependence of this coefficient on, separately, permittivity and conductivity contrasts (*ibid.*, p. 252). This is a common approach to get around the fact that the full version of the radar reflection coefficient involves complex quantities (Dowdeswell and

https://doi.org/10.5194/tc-2020-9
Preprint. Discussion started: 6 February 2020
© Author(s) 2020. CC BY 4.0 License.

40 Evans, 2004, eq. 7; Bradford, 2007). Whereas radar waves can typically transmit much energy through weak englacial reflectors and provide information on the structure over a large range of ice thicknesses, the radar reflectivity of the ice bed offers basically the only insight from radar surveys into the nature of geologic materials underlying ice masses. This is because sub-ice environments are typically not imaged directly by ice penetrating radars (Plewes and Hubbard, 2001). Rather, inferences about sub-ice
45 conditions, e.g., the presence or absence of subglacial water, are drawn from the lateral variations in radar bed reflectivity (e.g., Catania et al., 2003).

Here, we build on the pioneering work of Stratton (1941) to propose a version of the specular radar amplitude reflection coefficient, which retains both real permittivity and conductivity of the two media
50 that are separated by the reflecting interface. We then illustrate how this development can improve glaciological interpretations of radar reflections.

2 Background on Plane Electromagnetic Waves

In general, mathematical treatment of propagation and reflection of electromagnetic (henceforth EM) waves includes three fundamental properties of the media through which EM waves propagate:
55 dielectric permittivity, ε; electric conductivity, σ; and magnetic permeability, μ. Maxwell's equations for EM waves in homogeneous and isotropic media illustrate the role of these properties in EM wave propagation (Stratton, 1941, p. 268):

$$\nabla \times \boldsymbol{E} + \mu \frac{\partial \boldsymbol{H}}{\partial t} = 0 \quad (1a)$$

$$\nabla \times \boldsymbol{H} - \varepsilon \frac{\partial \boldsymbol{E}}{\partial t} - \sigma \boldsymbol{E} = 0 \quad (1b)$$

https://doi.org/10.5194/tc-2020-9
Preprint. Discussion started: 6 February 2020
© Author(s) 2020. CC BY 4.0 License.

$$\nabla \cdot \boldsymbol{H} = 0 \quad (1c)$$

$$\nabla \cdot \boldsymbol{E} = 0 \quad (1d)$$

where $\boldsymbol{E}$ denotes the electric field intensity vector, $\boldsymbol{H}$ is the magnetic field intensity vector, and t is time. Magnetic permeability and dielectric permittivity are associated with time derivatives of the magnetic and electric field intensities, respectively (Eq. 1ab). Their values are never zero, even in free space, and they can be thought of as an analog for elastic constants used in description of seismic wave propagation. The free space values of $\varepsilon_o = 8.8541878128 \times 10^{-12}$ $s^2H^{-1}m^{-1}$ and $\mu_o = 1.25663706212 \times 10^{-6}$ H m^{-1} are used in physics and geophysics as reference quantities, so that, for instance, relative dielectric permittivity, sometimes also referred to as the specific inductive capacity, is defined as $\varepsilon_r = \varepsilon / \varepsilon_o$. In contrast to magnetic permeability and dielectric permittivity, electric conductivity can be zero (e.g., free space) or negligibly small (e.g., glacier ice). In such media, EM waves can propagate (nearly) without loss of amplitude since conductive electric currents, represented in Eq. (1b) by the third term on the left-hand side, provide the physical mechanism for EM wave attenuation. It is worth noting that in geophysical literature it is often customary to substitute electrical resistivity, ρ, expressed in Ωm, for electrical conductivity, σ, with units of S m^{-1}. It is straightforward to switch between the two since one is simply the reciprocal of the other, such that $\rho = 1/\sigma$, or vice versa. Another noteworthy fact is that most materials on and near the Earth's surface, including most common minerals, rocks, ice, and water, have magnetic permeability that is not significantly different from that of free space, μ_o, except for a small subset of minerals that are not very abundant (O'Reilly, 1976; Keller, 1988). Later this will become important because it will enable us to eliminate magnetic permeability from the equations describing radar wave reflection, in which it appears both in the numerator and denominator. This will

https://doi.org/10.5194/tc-2020-9
Preprint. Discussion started: 6 February 2020
© Author(s) 2020. CC BY 4.0 License.

simplify the problem of radar reflection to a function of just two material properties: electrical conductivity and dielectric permittivity.

Before focusing on analyses of EM wave reflection, we note that Stratton (1941, section 5.2) proposed solutions describing propagation and reflection of harmonic plane waves in the homogeneous and isotropic media by using a complex propagation constant, $\boldsymbol{k}$, defined as (*ibid,* eq. 30):

$$\boldsymbol{k} = \alpha + \boldsymbol{i}\beta \tag{2}$$

where α is the phase constant and β is the attenuation factor while $\boldsymbol{i}$ is the standard imaginary unit, such that $\boldsymbol{i}^2 = -1$. We note that throughout this paper, we will use bold type for symbols designating complex quantities. The complex propagation constant plays a crucial role in Stratton's expressions for the reflection coefficient. It should be noted that in geophysical literature, the meaning of symbols α and β is sometimes switched, so that the former is the attenuation factor (e.g., Knight, 2001, p. 231). Since Stratton's work provides the basis for our analyses, we will keep using his terminology here. The two components of the propagation constant are given by (Stratton, 1941, eqs. 48 and 49):

$$\alpha = \omega\left[\frac{\mu\varepsilon}{2}\left(\sqrt{1+\frac{\sigma^2}{\varepsilon^2\omega^2}}+1\right)\right]^{1/2} \tag{3a}$$

$$\beta = \omega\left[\frac{\mu\varepsilon}{2}\left(\sqrt{1+\frac{\sigma^2}{\varepsilon^2\omega^2}}-1\right)\right]^{1/2} \tag{3b}$$

where ω is the angular frequency, related to the linear frequency f through $\omega = 2\pi f$, and all other symbols have been already defined. It is of paramount importance to our later analyses to note after Stratton (1941, p. 276) "…that α and β must be real." Hence, the only imaginary part of the complex

https://doi.org/10.5194/tc-2020-9
Preprint. Discussion started: 6 February 2020
© Author(s) 2020. CC BY 4.0 License.

propagation constant, $\boldsymbol{k}$, is due to the term $\boldsymbol{i\beta}$ on the right-hand side of Eq. (2). Although the material properties such as electrical permittivity and conductivity may themselves be expressed as complex quantities (e.g., Bradford, 2007), Eq. (3ab) require real values of all three material parameters, ε, σ, μ, applicable at a specific angular frequency, ω (Stratton, 1941, p. 511).

Equations (3ab) reveal three general modes of behavior, governed by the value of the ratio $\sigma/(\varepsilon\omega)$ (Figure 1). In the simplest, low-loss, case, when electrical conductivity is either zero or negligible ($\sigma << \varepsilon\omega$), the phase and attenuation factors simplify to:

$$\alpha = \omega\sqrt{\mu\varepsilon} \quad (4a)$$

$$\beta = 0 \quad (4b)$$

and the propagation constant, which is no longer a complex quantity since $\beta = 0$, becomes:

$$k = \alpha = \omega\sqrt{\mu\varepsilon} \quad (4c)$$

This assumption is often made in glaciological and geophysical radar interpretation (e.g., Knight, 2001; Plewes and Hubbard, 2001; Dowdeswell and Evans, 2004) and it is certainly justified for most glacier ice, which has sufficiently low conductivity at a wide range of frequencies (e.g., Stillman et al., 2013).

Glacier ice, and other materials for which $\sigma << \varepsilon\omega$, can be classified as good dielectrics with low loss with respect to propagation of EM waves (Figure 1). At the opposite end of the spectrum, when $\sigma >> \varepsilon\omega$, the material can be classified as high-loss, poor dielectric medium (Figure 1) and Eq. (3ab) simplify to:

$$\alpha = \beta = \sqrt{\frac{\mu\omega\sigma}{2}} \quad (5a)$$

https://doi.org/10.5194/tc-2020-9
Preprint. Discussion started: 6 February 2020
© Author(s) 2020. CC BY 4.0 License.

and the complex propagation constant becomes:

$$\boldsymbol{k} = \alpha(1+\boldsymbol{i}) = \beta(1+\boldsymbol{i}) = \sqrt{\frac{\mu\omega\sigma}{2}}(1+\boldsymbol{i}) \qquad (5b)$$

The full versions of Eq. (2) and (3ab) are, thus, only needed when dealing with the transitional region corresponding approximately to conditions when $0.1\varepsilon\omega < \sigma < 10\varepsilon\omega$. In Figure 1, these limits correspond to ca. 5-10% error in the low-loss and high-loss values of α and β, Eq. (4ab) and (5a), as compared to their values calculated using Eq. (3ab). In practical applications of radar reflectivity investigations, the challenge, of course, is that it may be impossible to know *a priori* what the electrical conductivity of the target material is and to decide which form of the propagation constants is applicable.

3 The Low-Loss Assumption and Its Limitations

As can be easily gleaned from Eq. (4abc), the most convenient simplification of Eq. (2) and (3ab) results from the low-loss assumption, $\sigma << \varepsilon\omega$, because the propagation constant is then no longer a complex number and one material property, the electrical conductivity, can be completely eliminated from further consideration. As mentioned above, this assumption is a reasonable one for glacier ice. However, it cannot be necessarily assumed to generally hold for subglacial materials such as saturated bedrock and sediments or for marine accreted ice of ice shelves.

Figure 2 allows us to verify if the range of electrical conductivity and relative permittivity for common geologic materials justifies the low-loss assumption. For illustration purposes, we use three different

https://doi.org/10.5194/tc-2020-9
Preprint. Discussion started: 6 February 2020
© Author(s) 2020. CC BY 4.0 License.

linear frequencies, f, of 1, 10, and 100 MHz, which are representative of the range of linear frequencies used in glaciology, planetary science, and ground penetrating radar (GPR) investigations (e.g., Jacobel and Raymond, 1984; Catania et al., 2003; Bradford, 2007; Holt et al., 2008; Mouginot et al., 2014). As a reminder, the angular frequency is related to the linear frequency by: $\omega = 2\pi f$. The relative permittivity considered in Figure 2 spans that expected for common minerals and rocks in dry conditions at the low end to 100% liquid water by volume at the high end (Midi et al., 2014; Josh and Clennell, 2015). For each of the considered frequencies, the range of electrical conductivities for which neither the low-loss, nor the high-loss, assumption is truly justified covers about one order of magnitude. The exact conductivity values falling within this range are dependent on relative permittivity. For instance, for 100 MHz linear frequency, the low-loss limit corresponds to conductivity of ca. 0.01 S m^{-1} (resistivity of ca. 100 Ωm) for $\varepsilon_r = 5$, typical for dry minerals and rocks (e.g, Josh and Clennell, 2015), but is an order of magnitude higher ($\sigma = 0.1$ S m^{-1} and $\rho = 10$ Ωm) for $\varepsilon_r = 55$, which would be expected either for clay-poor sediments with very high water content or saturated clay-rich sediments (Arcone et al., 2008; Josh and Clennell, 2015).

Most common minerals have by themselves negligibly small electrical conductivity at pressures and temperatures prevailing near the surface of the Earth, except for metallic minerals and minerals exhibiting semiconductive behavior, like sulfides, oxides, and graphite (e.g., Keller, 1998). As embodied in the empirical Archie's law, the bulk electrical conductivity of sediments and rocks is mainly due to electrolytic conduction associated with the presence of liquid water and solutes in pore

https://doi.org/10.5194/tc-2020-9
Preprint. Discussion started: 6 February 2020
© Author(s) 2020. CC BY 4.0 License.

160 spaces and fractures (Archie, 1942). When re-written in terms of electrical conductivity, the original Archie's relation (Archie, 1942, eq. 3) becomes:

$$\sigma = \sigma_w \phi^m \quad (6)$$

where σ_w is the conductivity of pore fluid, ϕ is the porosity, expressed as a volume fraction of pore spaces, and m is the empirical cementation exponent. This relationship was originally developed for
165 clean sandstone and is less applicable to fine-grained, particularly clay-bearing, rocks and sediments for which surface conduction becomes important (Ruffet et al., 1995). This long-known conductive effect (Smoluchowski, 1918), represents an enhancement of electrolytic conduction near charged solid surfaces and its magnitude tends to scale with the specific surface area of sediments (e.g., Arcone et al., 2008; Josh and Clennel, 2015).

170

Overall, the low-loss assumption is less likely to be applicable in three general types of geologic materials: (1) ones containing sufficient concentration of conductive minerals (e.g., Hammond and Sprenke, 1981), (2) sediments and rocks saturated with high conductivity fluids, and (3) saturated clay-bearing rocks and sediments. If we take the low-loss conductivity limits for 100 MHz frequency from
175 Figure 2, 0.01-0.1 S m^{-1}, and apply them to the compilation of electrical conductivity for geologic materials in figure 1 of Ruffet et al. (1995) the low-loss assumption is questionable for a wide range of materials, including shales, sandstones, coal, metamorphic rocks, igneous rocks as well as graphite and sulfides. This simplifying assumption is even more generally suspect for lower frequencies, such as 1 and 10 MHz in Figure 2.

180

https://doi.org/10.5194/tc-2020-9
Preprint. Discussion started: 6 February 2020
© Author(s) 2020. CC BY 4.0 License.

The compilation data in figure 1 of Ruffet et al. (1995) can be criticized as being overly generalized and we turn now to some specific relevant studies. In our regional helicopter-borne time-domain EM survey of liquid-bearing subglacial and sub-permafrost materials performed in McMurdo Dry Valley region in Antarctica we mostly observed electrical resistivities of 1-100 Ωm (σ = 0.01-1 S m^{-1}) (Dugan et al., 2015; Mikucki et al., 2015; Foley et al., 2016; Foley et al., 2019). Extensive regional DC and EM surveys of Pleistocene glacial sequences in Denmark and Germany yielded resistivities in the same range of values, except for clean outwash sand and gravel which tend to be more resistive (Steuer et al., 2009; Jorgensen et al., 2012). Hence, these results of regional resistivity surveys in modern and past glacial environments also support the contention that the low-loss assumption is not generally applicable to geologic materials expected beneath glaciers and ice sheets, or in post-glacial landscapes. Although our focus here is on glacial environments, we conjecture based on our review of available constraints that it may be similarly problematic to make such blanket low-loss assumption in GPR investigations of reflectors in other saturated sediments (e.g., Bradford, 2007).

4 General and Simplified Forms of the Radar Reflection Coefficient

In order to illustrate the general form of the radar reflection coefficient we start with the expression derived by Stratton (1941, chapter 9) for a reflecting interface separating two homogeneous and isotropic half spaces characterized by three scalar material properties each: ε_1, ε_2, σ_1, σ_2, μ_1, μ_2 (Figure 3). We limit ourselves to considering specular reflection of a plane wave approaching the interface at normal incidence from medium 1 towards medium 2 (adapted from Stratton, 1941, p. 512, eq. 11):

$$\boldsymbol{r} \equiv \frac{\boldsymbol{E_r}}{\boldsymbol{E_o}} = \frac{\mu_2 \boldsymbol{k_1} - \mu_1 \boldsymbol{k_2}}{\mu_2 \boldsymbol{k_1} + \mu_1 \boldsymbol{k_2}} \quad (7a)$$

https://doi.org/10.5194/tc-2020-9
Preprint. Discussion started: 6 February 2020
© Author(s) 2020. CC BY 4.0 License.

where $\boldsymbol{r}$ is the complex reflection coefficient, defined as the complex intensity of the reflected wave, $\boldsymbol{E_r}$, normalized by the complex intensity of the incident wave, $\boldsymbol{E_o}$. The materials on both sides of the reflecting interface are characterized by complex propagation constants, $\boldsymbol{k_1}$ and $\boldsymbol{k_2}$, which are related to the respective material constants characterizing the media (i.e., ε_1, ε_2, σ_1, σ_2, μ_1, μ_2) through Eq. (2) and (3ab) (Figure 3).

At this point we will simplify Eq. (7a) by assuming that both of the media have the magnetic permeability of free space, as it is reasonable to do for most rocks and minerals at temperatures and pressures near the surface of the Earth. With this simplification Eq. (7a) becomes:

$$\boldsymbol{r} = \frac{\boldsymbol{k_1}-\boldsymbol{k_2}}{\boldsymbol{k_1}+\boldsymbol{k_2}} = \frac{\alpha_1+\boldsymbol{i}\beta_1-\alpha_2-\boldsymbol{i}\beta_2}{\alpha_1+\boldsymbol{i}\beta_1+\alpha_2+\boldsymbol{i}\beta_2} = \frac{(\alpha_1-\alpha_2)+\boldsymbol{i}(\beta_1-\beta_2)}{(\alpha_1+\alpha_2)+\boldsymbol{i}(\beta_1+\beta_2)} \quad (7b)$$

where we have expanded the right-hand side of this equation using the complex propagation constants, $\boldsymbol{k_1}$ and $\boldsymbol{k_2}$, (Eq. 2) for both media. The real amplitude reflection coefficient, r, can be expressed as the absolute value of the complex vector $\boldsymbol{r}$:

$$r = |\boldsymbol{r}| = \sqrt{\frac{(\alpha_1-\alpha_2)^2+(\beta_1-\beta_2)^2}{(\alpha_1+\alpha_2)^2+(\beta_1+\beta_2)^2}} \quad (8)$$

where the absolute value is, by definition, the Pythagorean length of the complex vector, $\boldsymbol{r}$, in the complex plane (Argand Diagram).

The power reflection coefficient, R, is the square of Eq. (8) (Stratton, 1941, p. 512, eq. 12):

$$R = \frac{(\alpha_1-\alpha_2)^2+(\beta_1-\beta_2)^2}{(\alpha_1+\alpha_2)^2+(\beta_1+\beta_2)^2} \quad (9)$$

https://doi.org/10.5194/tc-2020-9
Preprint. Discussion started: 6 February 2020
© Author(s) 2020. CC BY 4.0 License.

220 It is worth noting that Eq. (8) and (9) are, on their own, underconstrained. At least in glaciology, one can put reasonable constraints on the electrical conductivity and permittivity of ice, σ_1 and ε_1 (e.g., Stillman et al., 2013), which, in this example, corresponds to the medium 1 through which the incident wave is propagating towards the reflecting interface (Figure 3). The two unknowns are then the electrical conductivity and permittivity, σ_2 and ε_2, of the medium underlying ice. Additional constraint
225 can be gained from the tangent of the phase shift angle of the reflected wave, given by (Stratton, 1941, p. 513, eq. 15):

$$\tan(\varphi) = \frac{2(\alpha_2\beta_1 - \alpha_1\beta_2)}{(\alpha_1^2 + \beta_1^2) - (\alpha_2^2 + \beta_2^2)} \quad (10)$$

So, if radar reflectivity and phase shift, φ, can be measured accurately enough then, at least in principle, Eq. (8) and (10) represent a system two equations with two unknowns, σ_2 and ε_2. However, we will later
230 illustrate limitations of this approach that are related to the fact that in both limiting regimens, the low-loss and the high-loss one, the tangent of the phase shift angle is small.

Let us now examine the two limiting cases of Eq. (9), first when the sub-ice material is low loss and then when it is high loss. In the first case, $\sigma_2 << \varepsilon_2\omega$, we substitute Eq. (4ab) for α_1, α_2, and β_1, β_2 in Eq.
235 (8) and obtain:

$$r = \sqrt{\frac{(\alpha_1 - \alpha_2)^2}{(\alpha_1 + \alpha_2)^2}} = \frac{\alpha_1 - \alpha_2}{\alpha_1 + \alpha_2} = \frac{\sqrt{\varepsilon_1} - \sqrt{\varepsilon_2}}{\sqrt{\varepsilon_1} + \sqrt{\varepsilon_2}} \quad (11)$$

The reflection coefficient simplifies to a function of only permittivities of ice, ε_1, and the sub-ice geologic material, ε_2. This is an encouraging result because it agrees with a widely used form of radar reflection coefficient in the case of an interface between two perfect dielectrics (e.g., Knight, 2001). The

https://doi.org/10.5194/tc-2020-9
Preprint. Discussion started: 6 February 2020
© Author(s) 2020. CC BY 4.0 License.

tangent of the phase shift angle (Eq. 10) is always zero for the low-loss case but the phase shift angle is either zero, when r values are positive, or 180º when they are negative.

For the second case, we assume that ice (medium 1 in Figure 3) is still a lossless dielectric but that the sub-ice medium is high loss, $\sigma_2 >> \varepsilon_2\omega$, so that we use Eq. (4ab) for α_1, β_1, and Eq. (5a) for α_2, β_2 in Eq. (8):

$$r = \sqrt{\frac{(\alpha_1-\alpha_2)^2+{\alpha_2}^2}{(\alpha_1+\alpha_2)^2+{\alpha_2}^2}} = \sqrt{\frac{\omega\varepsilon_1-\sqrt{2\varepsilon_1\omega\sigma_2}+\sigma_2}{\omega\varepsilon_1+\sqrt{2\varepsilon_1\omega\sigma_2}+\sigma_2}} \approx \sqrt{\frac{\sigma_2-\sqrt{2\varepsilon_1\omega\sigma_2}}{\sigma_2+\sqrt{2\varepsilon_1\omega\sigma_2}}} \quad (12)$$

where the final, approximate, expression on the right-hand side is taking advantage of the fact that, under the high-loss assumption, $\sigma_2 >> \varepsilon_1\omega$ given that the permittivity of ice is low (Stillman et al., 2013). As shown by Eq. (12), the high-loss version of the reflection coefficient is sensitive to the angular frequency, ω, the permittivity of ice, ε_1, and electrical conductivity of the sub-ice material, σ_2.

5 Discussion

Figure 4 shows the full version of the amplitude reflection coefficient (Eq. 8) plotted for the case of 100 MHz linear frequency and a range of relative permittivities (in this case $\varepsilon_r = \varepsilon_2/\varepsilon_o$) and electrical conductivities for the sub-ice material. The family of horizontal line segments on the left corresponds to the case of lossless dielectric media being present beneath ice. These line segments can be approximated by Eq. (11), which is commonly used in glaciology and GPR studies to make inferences about the nature of geologic materials. Due to the fact that common minerals have relatively low relative permittivity (5-10) and liquid water has very high relative permittivity (Midi et al., 2014), the

https://doi.org/10.5194/tc-2020-9
Preprint. Discussion started: 6 February 2020
© Author(s) 2020. CC BY 4.0 License.

strength of the basal reflection coefficient is often interpreted solely as the function of water content. This is also a common practice in GPR investigations of interfaces between sediment layers (e.g., Stoffregen et al., 2002). In glaciology and planetary science, for instance, bright radar reflectors have been used in the search for subglacial lakes on Earth and Mars because open water bodies beneath ice should be the most reflective subglacial materials, at least in the low loss regimen described by Eq. (11) (Plewes and Hubbard, 2001; Dowdeswell and Evans, 2004; Orosei et al., 2018).

Starting at electrical conductivity of 0.01-0.1 S m^{-1} (resistivity of 10-100 Ωm), the reflection coefficient for 100MHz frequency, becomes increasingly more dependent on the conductivity than on the permittivity of the sub-ice material. At conductivities greater than 0.1 S m^{-1} (resistivity of 10 Ωm), the coefficient is for all practical purposes independent of relative permittivity of subglacial materials and rises in value above its high value of 0.67 characterizing the ice-above-water scenario under lossless conditions. This means that high conductivity subglacial materials can appear significantly brighter than subglacial lakes filled with fresh meltwater. Such high conductivity materials can include seawater- or brine-saturated sediments and bedrock (Foley et al., 2015, table 2) as well as clay-bearing sediments or bedrock saturated with natural waters of any reasonable conductivity. Large parts of the Antarctic ice sheet are underlain by clay-rich subglacial tills, which may contain over 30% clay (Tulaczyk et al., 1998; Studinger et al., 2001; Tulaczyk et al., 2014; Hodson et al., 2016).

The effect of electrical conductivity of subglacial materials on basal radar reflectivity may be responsible for some past puzzling glaciological radar results. For instance, Christianson et al. (2012)

https://doi.org/10.5194/tc-2020-9
Preprint. Discussion started: 6 February 2020
© Author(s) 2020. CC BY 4.0 License.

used a 5 MHz center frequency radar to perform extensive mapping of basal reflectivity around Subglacial Lake Whillans. They failed to find a relationship between the outline of the lake inferred from satellite altimetry and the observed pattern of basal radar reflectivity. Subsequent drilling found very clay-rich sediments in the region (Tulaczyk et al., 2014; Hodson et al., 2016) and such subglacial sediments can be conductive enough to produce radar reflectivity that is the same, or higher, than reflectivity from an ice-lake interface (e.g., Arcone et al., 2008). This is particularly the case for low frequency radar waves with center frequency of 5MHz, for which only subglacial materials that are less conductive than ca. 0.01-0.001 S m^{-1} (resistivity of 100-1000 Ωm), depending on permittivity, will meet the criterion of a low-loss material.

In the same general part of Antarctica, MacGregor et al. (2011) mapped basal reflectivity across the grounding zone of Whillans Ice Stream using a 2 MHz radar. Their survey found no clear increase in radar reflectivity across the grounding line, where the ice base goes from being underlain by saturated sediments to floating on seawater. If one interprets this setting in the context of the low-loss assumption (Eq. 11), basal reflectivity should be higher over seawater than sediments (Arcone et al., 2008; Midi et al., 2014). However, Eq. (12) solved for a 2MHz linear frequency (detailed results not shown here) shows a high reflection coefficient of ca. 0.9 for all subglacial materials with conductivity higher than 0.05 S m^{-1} (resistivity of 20 Ωm). Since seawater has electrical conductivity of ca. 0.25 S m^{-1} (4 Ωm) and the clay rich subglacial sediments in the region can have conductivity >0.05 S m^{-1} (<20 Ωm) (Arcone et al., 2008; Josh and Clennel, 2015), the radar survey of MacGregor et al. (2011) may have encountered a problem arising from the high-loss end member of the reflection coefficient (Eq. 12). In

https://doi.org/10.5194/tc-2020-9
Preprint. Discussion started: 6 February 2020
© Author(s) 2020. CC BY 4.0 License.

this regimen, the reflection coefficient is no longer sensitive to relative permittivity so that transition from saturated sediments to pure water no longer increases the reflection coefficient. At the same time, the value of reflectivity calculated from Eq. (12) changes only slightly with changes in already high electrical conductivity so that differences in conductivity between seawater and clay-rich sediments may be too small to be detectable in noisy radar reflection data.

One piece of observational evidence, the phase shift of the reflected wave, can be used, at least under some circumstances, to independently check if electrical conductivity of the sub-ice material plays a role in controlling basal reflectivity. Figure 5 illustrates that as the electrical conductivity becomes either very large or very small, the phase shift angle is small in either case, thus limiting the ability to use the phase angle to determine if strong radar bed reflectivity is due to high permittivity or conductivity contrasts. Another potentially helpful approach is to take advantage of the fact that the low-loss reflection coefficient is frequency independent (Eq. 11) but that the high-loss version retains frequency dependence (Eq. 12). Within the typical range of linear radar frequencies used in glaciology (1-100MHz), this frequency sensitivity of the reflection coefficient is the highest at low frequencies (1-10 MHz) and at relatively low conductivities (0.001-0.1 S m^{-1}) (Figure 6). As the conductivity of subglacial materials approaches that of highly conductive clay-rich sediments and seawater (>0.1 S m^{-1}), the amplitude reflection coefficient becomes increasingly less sensitive to frequency. Multi-frequency mapping of basal radar reflectivity may, thus provide, a useful constraint on the presence or absence of conductive materials beneath ice. However, just like in the case of the phase shift angle, it is an approach that will work only for some range of subglacial conductivities.

https://doi.org/10.5194/tc-2020-9
Preprint. Discussion started: 6 February 2020
© Author(s) 2020. CC BY 4.0 License.

6 Conclusions

The assumption that radar reflection is generated at an interface between two lossless dielectric materials is certainly appealing, because it simplifies the problem to a contrast solely in permittivity (Eqs. 11) and eliminates the dependence of reflectivity on radar frequency and electrical conductivity. However, our examination of the criterion for the lossless conditions, $\sigma >> \varepsilon\omega$, indicates that it is unrealistic for a wide range of common geologic materials for the range of linear radar frequencies (1-100 MHz) used in glaciology, planetary sciences, and GPR investigations. This is particularly the case for the low frequency radars (e.g., 2-5 MHz center frequency) used in glaciology and planetary science, for which even materials with conductivity as low as ca. 0.0001-0.001 S m^{-1} (1,000-10,000 Ωm) are too high for the lossless criterion to be applicable (Fig. 2). But even at the high end of frequencies (ca. 100 MHz), a number of geologic materials can have high enough conductivity, 0.01-1 S m^{-1} (1-100 Ωm) for it to matter in radar reflectivity. In the absence of *a priori* constraints on the electrical conductivity of target materials, -interpretations of radar interface reflectivity should be made based on the full form of the reflection coefficient, which retains the dependence on conductivity and frequency, in addition to permittivity (Eq. 8). Since Eq. (8) contains at least two unknown material properties, the permittivity and the conductivity of the target material (e.g., subglacial material), it is possible to gain additional constraints using either the phase shift of the reflected way (Eq. 10) or the frequency dependence of the reflection coefficient (Eqs. 8, 12). In some cases, for instance when ice is in contact with a body of water, sub-ice permittivity is known and the basal radar reflectivity can be used to directly constrain the sub-ice electrical

https://doi.org/10.5194/tc-2020-9
Preprint. Discussion started: 6 February 2020
© Author(s) 2020. CC BY 4.0 License.

conductivity, σ_2. This will allow estimating the salinity of subglacial lakes on Earth and sub-ice oceans on icy planetary bodies.

345

7 Team list

Slawek M. Tulaczyk and Neil T. Foley at the Department of Earth and Planetary Sciences, University of California, Santa Cruz.

8 Author contributions

350 Slawek M. Tulaczyk designed this research, performed analyses, and wrote the manuscript. Neil T. Foley co-designed this research and contributed to manuscript writing and editing.

9 Competing interests

The authors declare that they have no conflict of interest.

355

10 Acknowledgments

This material is based upon work supported by the National Science Foundation under Grant No. 1644187. The content of this paper is the sole responsibility of the authors.

11. References

360 Archie, G.E.: The electrical resistivity log as an aid in determining some reservoir characteristics, Trans. AIME, 146(01), 54-62, 1942.

https://doi.org/10.5194/tc-2020-9
Preprint. Discussion started: 6 February 2020
© Author(s) 2020. CC BY 4.0 License.

Arcone, S., Grant, S., Boitnott, G. and Bostick, B.: Complex permittivity and clay mineralogy of grain-size fractions in a wet silt soil, Geoph., 73(3), J1-J13, 2008.

365

Aglyamov, Y., Schroeder, D.M. and Vance, S.D.: Bright prospects for radar detection of Europa's ocean, Icarus, 281, 334-337, 2017.

Bierson, C.J., Phillips, R.J., Smith, I.B., Wood, S.E., Putzig, N.E., Nunes, D. and Byrne, S.:
370 Stratigraphy and evolution of the buried CO2 deposit in the Martian south polar cap, Geoph. Res. Lett., 43(9), 4172-4179, 2016.

Bradford, J.H.: Frequency-dependent attenuation analysis of ground-penetrating radar data, Geop., 72(3), J7-J16, 2007.

375

Catania, G.A., Conway, H.B., Gades, A.M., Raymond, C.F. and Engelhardt, H.: Bed reflectivity beneath inactive ice streams in West Antarctica, Ann. Glac., 36, 287-291, 2003.

Christianson, K., Jacobel, R.W., Horgan, H.J., Anandakrishnan, S. and Alley, R.B.: Subglacial Lake
380 Whillans—Ice-penetrating radar and GPS observations of a shallow active reservoir beneath a West Antarctic ice stream, EPSL, 331, 237-245, 2012.

https://doi.org/10.5194/tc-2020-9
Preprint. Discussion started: 6 February 2020
© Author(s) 2020. CC BY 4.0 License.

Chyba, C.F., Ostro, S.J. and Edwards, B.C.: Radar detectability of a subsurface ocean on Europa, Icarus, 134(2), 292-302, 1998.

385

Dowdeswell, J.A. and Evans, S.: Investigations of the form and flow of ice sheets and glaciers using radio-echo sounding, Rep. Prog. Phys., 67(10), 1821-1861, 2004.

Dugan, H.A., Doran, P.T., Tulaczyk, S., Mikucki, J.A., Arcone, S.A., Auken, E., Schamper, C. and
390 Virginia, R.A.: Subsurface imaging reveals a confined aquifer beneath an ice-sealed Antarctic lake, Geoph. Res. Lett., 42(1), 96-103, 2015.

Foley, N., Tulaczyk, S., Auken, E., Schamper, C., Dugan, H., Mikucki, J., Virginia, R. and Doran, P.: Helicopter-borne transient electromagnetics in high-latitude environments: An application in the
395 McMurdo Dry Valleys, Antarctica, AEM resistivity in the Dry Valleys, Geoph., 81(1), WA87-WA99, 2016.

Foley, N., Tulaczyk, S., Auken, E., Grombacher, D., Mikucki, J., Foged, N., Myers, K., Dugan, H., Doran, P.T. and Virginia, R.A.: Mapping geothermal heat flux using permafrost thickness constrained
400 by airborne electromagnetic surveys on the western coast of Ross Island, Antarctica, Expl. Geoph., DOI: 10.1080/08123985.2019.1651618, 2019.

Glen, J.W. and Paren, J.G.: The electrical properties of snow and ice, J. Glac., 15(73), 15-38, 1975.

https://doi.org/10.5194/tc-2020-9
Preprint. Discussion started: 6 February 2020
© Author(s) 2020. CC BY 4.0 License.

405 Hammond, W.R. and Sprenke, K.F.: Radar detection of subglacial sulfides, Geoph., 56(6), 870-873, 1991.

Hodson, T.O., Powell, R.D., Brachfeld, S.A., Tulaczyk, S., Scherer, R.P. and Team, W.S.: Physical processes in Subglacial Lake Whillans, West Antarctica: inferences from sediment cores, EPSL, 444, 410 56-63, 2016.

Holt, J.W., Safaeinili, A., Plaut, J.J., Head, J.W., Phillips, R.J., Seu, R., Kempf, S.D., Choudhary, P., Young, D.A., Putzig, N.E. and Biccari, D.: Radar sounding evidence for buried glaciers in the southern mid-latitudes of Mars, Science, 322(5905), 1235-1238, 2008.

415

Jacobel, R. and Raymond, C.: Radio echo-sounding studies of englacial water movement in Variegated Glacier, Alaska, J. Glac., 30(104), 22-29, 1984.

Josh, M. and Clennell, B.: Broadband electrical properties of clays and shales: Comparative 420 investigations of remolded and preserved samples, Geoph., 80(2), D129-D143, 2015.

Jørgensen, F., Scheer, W., Thomsen, S., Sonnenborg, T.O., Hinsby, K., Wiederhold, H., Schamper, C., Burschil, T., Roth, B., Kirsch, R. and Auken, E.; Transboundary geophysical mapping of geological

https://doi.org/10.5194/tc-2020-9
Preprint. Discussion started: 6 February 2020
© Author(s) 2020. CC BY 4.0 License.

elements and salinity distribution critical for the assessment of future sea water intrusion in response to sea level rise, Hydro. Earth Syst. Sci., 16(7), 1845-1862, 2012.

Keller, G.V.: Rock and mineral properties, Electrom. Meth. in App. Geoph., 1, 13-52, 1988.

Knight, R.: Ground penetrating radar for environmental applications, Ann. Rev. Earth and Planet. Sci., 29(1), 229-255, 2001.

MacGregor, J.A., Anandakrishnan, S., Catania, G.A. and Winebrenner, D.P.: The grounding zone of the Ross Ice Shelf, West Antarctica, from ice-penetrating radar. *Journal of Glaciology*, *57*(205), 917-928, 2011.

Midi, N.S., Sasaki, K., Ohyama, R.I. and Shinyashiki, N.: Broadband complex dielectric constants of water and sodium chloride aqueous solutions with different DC conductivities, IEEJ Trans. Elect. and Elect. Eng., 9(S1), S8-S12, 2014.

Mikucki, J.A., Auken, E., Tulaczyk, S., Virginia, R.A., Schamper, C., Sørensen, K.I., Doran, P.T., Dugan, H. and Foley, N.: Deep groundwater and potential subsurface habitats beneath an Antarctic dry valley, Nature Comms., 6, 6831, 2015.

https://doi.org/10.5194/tc-2020-9
Preprint. Discussion started: 6 February 2020
© Author(s) 2020. CC BY 4.0 License.

Mouginot, J., Rignot, E., Gim, Y., Kirchner, D. and Le Meur, E.: Low-frequency radar sounding of ice in East Antarctica and southern Greenland, Ann. Glac., 55(67), 138-146, 2014.

O'Reilly, W.: Magnetic minerals in the crust of the Earth. *Rep. Prog. Phys.*, *39*(9), 857-908, 1976.

Orosei, R., Lauro, S.E., Pettinelli, E., Cicchetti, A., Coradini, M., Cosciotti, B., Di Paolo, F., Flamini, E., Mattei, E., Pajola, M. and Soldovieri, F.: Radar evidence of subglacial liquid water on Mars, Science, 361(6401), 490-493, 2018.

Paren, J.G. and Robin, G.D.Q.: Internal reflections in polar ice sheets, J. Glac., 14(71), 251-259, 1975.

Peters, M.E., Blankenship, D.D. and Morse, D.L.: Analysis techniques for coherent airborne radar sounding: Application to West Antarctic ice streams, J. Geophys. Res.: Solid Earth, 110(B6), B06303, doi:10.1029/2004JB003222, 2005.

Plewes, L. A. and Hubbard, B.: A review of the use of radio-echo sounding in glaciology, Prog. Phys. Geog., 25(2), 203-236, 2001.

Ruffet, C., Darot, M. and Gueguen, Y.: Surface conductivity in rocks: a review, Surv. Geophys., 16(1), 83-105, 1995.

https://doi.org/10.5194/tc-2020-9
Preprint. Discussion started: 6 February 2020
© Author(s) 2020. CC BY 4.0 License.

465 Smoluchowski, M.V.: Versuch einer mathematischen Theorie der Koagulationskinetik kolloider Lösungen, Z. Phys. Chem., 92(1), 129-168, 1918.

Steuer, A., Siemon, B. and Auken, E.; A comparison of helicopter-borne electromagnetics in frequency- and time-domain at the Cuxhaven valley in Northern Germany. J. App. Geoph., 67(3), 194-205, 2009.

470

Stillman, D.E., MacGregor, J.A. and Grimm, R.E.; The role of acids in electrical conduction through ice, J. Geoph. Res.: Earth Surf., 118(1), 1-16, 2013.

Stoffregen, H., Zenker, T. and Wessolek, G.; Accuracy of soil water content measurements using
475 ground penetrating radar: comparison of ground penetrating radar and lysimeter data, J. Hydro., 267(3-4), 201-206, 2002.

Stratton, J.A.: Electromagnetic Theory, McGrow-Hill Book Company. *Inc., New York, and London*, 615pp, 1941.

480

Studinger, M., Bell, R.E., Blankenship, D.D., Finn, C.A., Arko, R.A., Morse, D.L. and Joughin, I.: Subglacial sediments: A regional geological template for ice flow in West Antarctica, Geoph. Res. Lett., 28(18), 3493-3496, 2001.

© Author(s) 2020. CC BY 4.0 License.

485 Tulaczyk, S., Kamb, B., Scherer, R.P. and Engelhardt, H.F.: Sedimentary processes at the base of a West Antarctic ice stream; constraints from textural and compositional properties of subglacial debris, J. Sed. Res., 68(3), 487-496, 1998.

Tulaczyk, S., Mikucki, J.A., Siegfried, M.R., Priscu, J.C., Barcheck, C.G., Beem, L.H., Behar, A.,
490 Burnett, J., Christner, B.C., Fisher, A.T. and Fricker, H.A.: WISSARD at Subglacial Lake Whillans, West Antarctica: scientific operations and initial observations, Ann. Glac., 55(65), 51-58, 2014.

12. Figure captions

Figure 1. Plot of the phase constant, α, and the attenuation constant, β, with the control parameter $\sigma/(\omega\varepsilon)$ on the horizontal axis and the pre-factor from Eq. (3ab), $\omega\mu^2\varepsilon^2/4$, on the vertical axis. The solid
495 lines show the full version of the expressions 3ab while the dashed horizontal line represents the lossless approximation of the phase constant, α (Eq. 4a). The dashed diagonal line gives the high-loss version of the phase and attenuation constants, α and β, which are equal to each other (Eq. 5a). The two grey regions on the left- and the right-hand side of the figure shows, the low loss and high loss conditions, respectively, in which the lossless and the high-loss solutions represent reasonable
500 approximations of the full solution.

Figure 2. Limits of lossless and high-loss conditions for three different linear radar frequencies, 1 MHz, 10 MHz, 100 MHz plotted in the conductivity-permittivity space.

https://doi.org/10.5194/tc-2020-9
Preprint. Discussion started: 6 February 2020
© Author(s) 2020. CC BY 4.0 License.

Figure 3. Schematic diagram showing the incident radar wave, E_o and solid arrow, the reflected wave, E_r and dashed line, as well as the transmitted wave, E_t and the dotted arrow. The horizontal thick line represents the reflective interface between materials 1 and 2, each characterized by three material properties: magnetic permeability, permittivity, and conductivity. This figure is adapted from Stratton (1941, figure 96).

Figure 4. The full version of the amplitude reflection coefficient (Eq. 8) plotted as a function of electrical conductivity, σ_2, and relative permittivity of the sub-ice material, $\varepsilon_r = \varepsilon_2/\varepsilon_o$. The relative permittivity is plotted at the increment of 5 between its assumed minimum value of 5 and the maximum value of 85. For ice, we use relative permittivity of 3.2 and the electrical conductivity of 10-5 S m^{-1} (Stillman et al., 2013). The reflection coefficient is given in fractional terms on the left axis and in decibels, to the precision of one tenth, on the right axis.

Figure 5. An equivalent plot to Figure 4 but here the tangent of the phase shift angle (Eq. 10) as a function of electrical conductivity and relative permittivity of the sub-ice material. The equivalent phase shift angles are given on the right axis. The material properties of ice are as assumed in Figure 4.

Figure 6. A plot demonstrating the frequency dependence of the high-loss version of the amplitude reflection coefficient (Eq. 12) for different values of electrical conductivity of the sub-ice material. The material properties of ice are as assumed in Figure 4.

https://doi.org/10.5194/tc-2020-9
Preprint. Discussion started: 6 February 2020
© Author(s) 2020. CC BY 4.0 License.

The Cryosphere
Discussions
Open Access
EGU

Figure 1

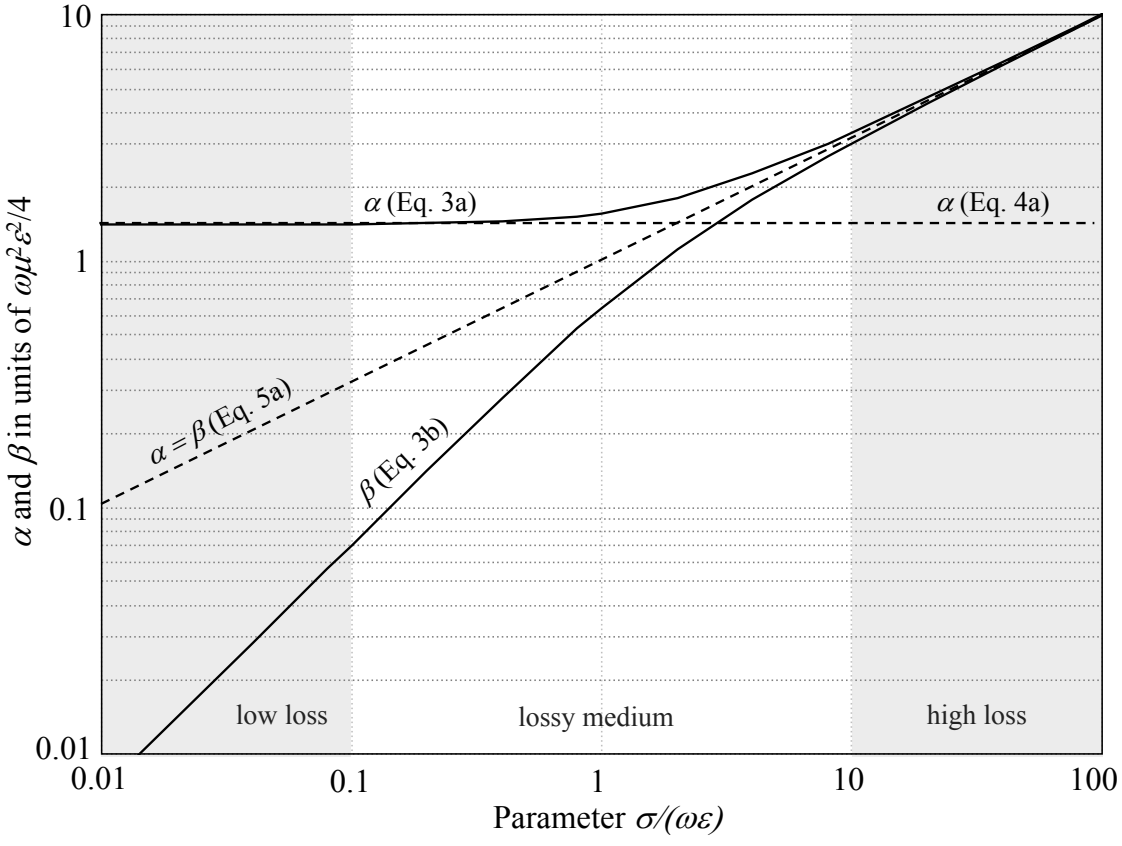

https://doi.org/10.5194/tc-2020-9
Preprint. Discussion started: 6 February 2020
© Author(s) 2020. CC BY 4.0 License.

The Cryosphere
Discussions
Open Access
EGU

Figure 2

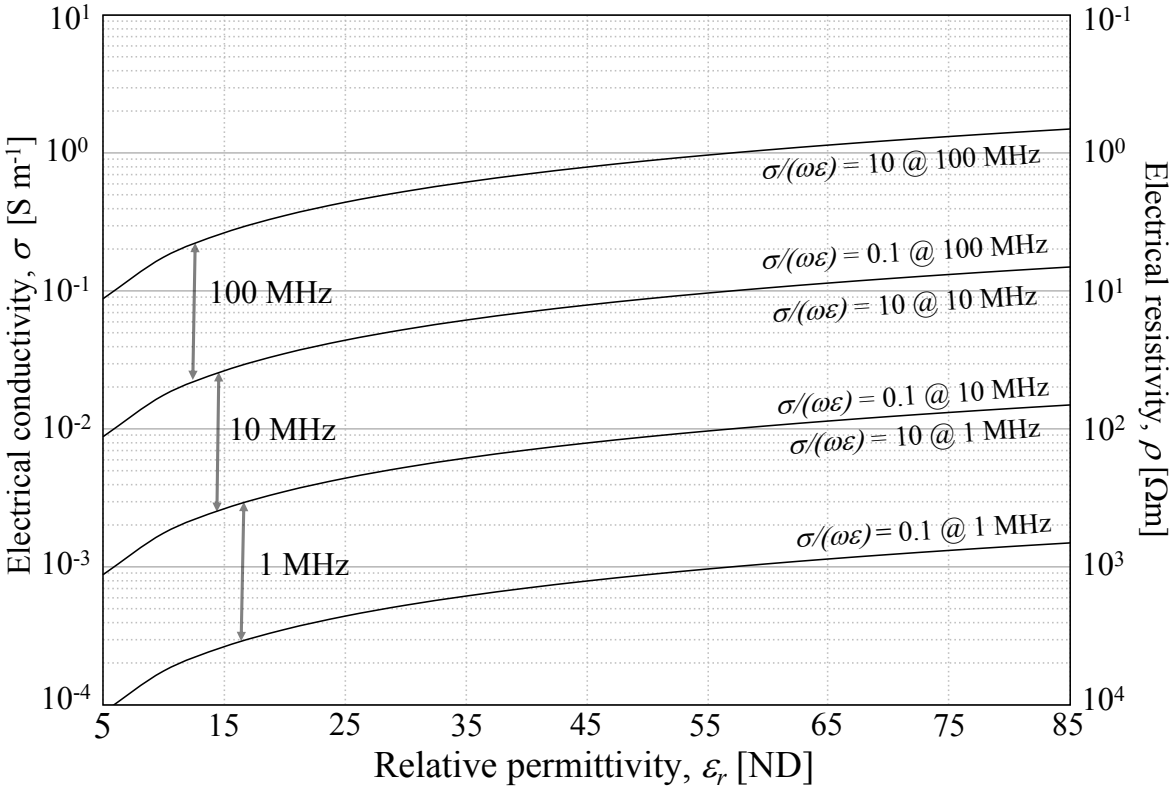

https://doi.org/10.5194/tc-2020-9
Preprint. Discussion started: 6 February 2020
© Author(s) 2020. CC BY 4.0 License.

The Cryosphere
Discussions
Open Access
EGU

Figure 3

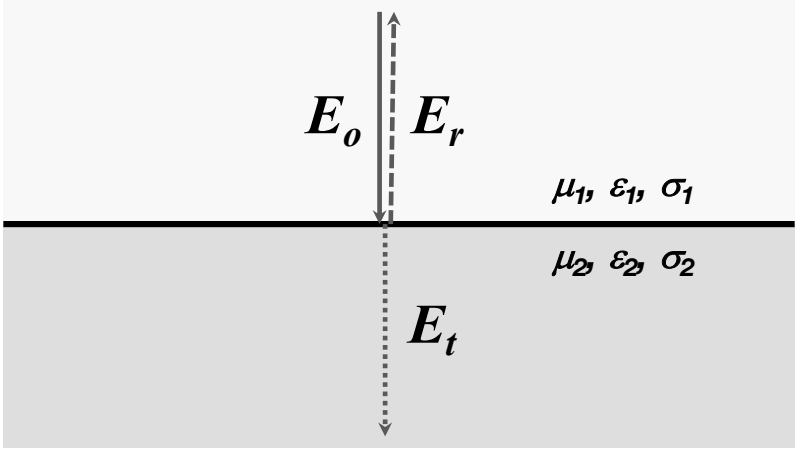

https://doi.org/10.5194/tc-2020-9
Preprint. Discussion started: 6 February 2020
© Author(s) 2020. CC BY 4.0 License.

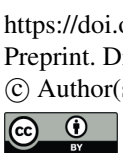

The Cryosphere
Discussions
Open Access
EGU

Figure 4

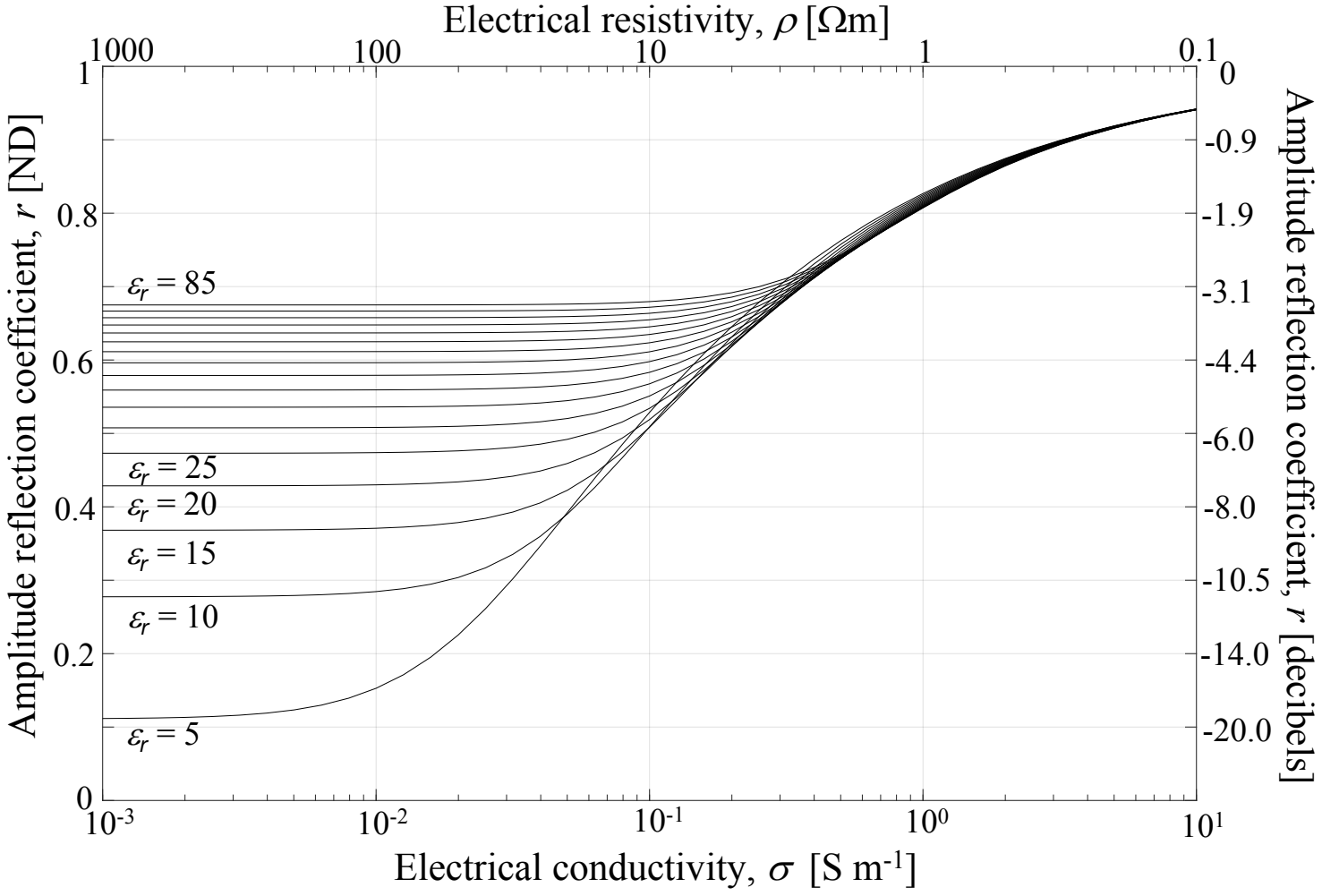

https://doi.org/10.5194/tc-2020-9
Preprint. Discussion started: 6 February 2020
© Author(s) 2020. CC BY 4.0 License.

The Cryosphere
Discussions
Open Access
EGU

Figure 5

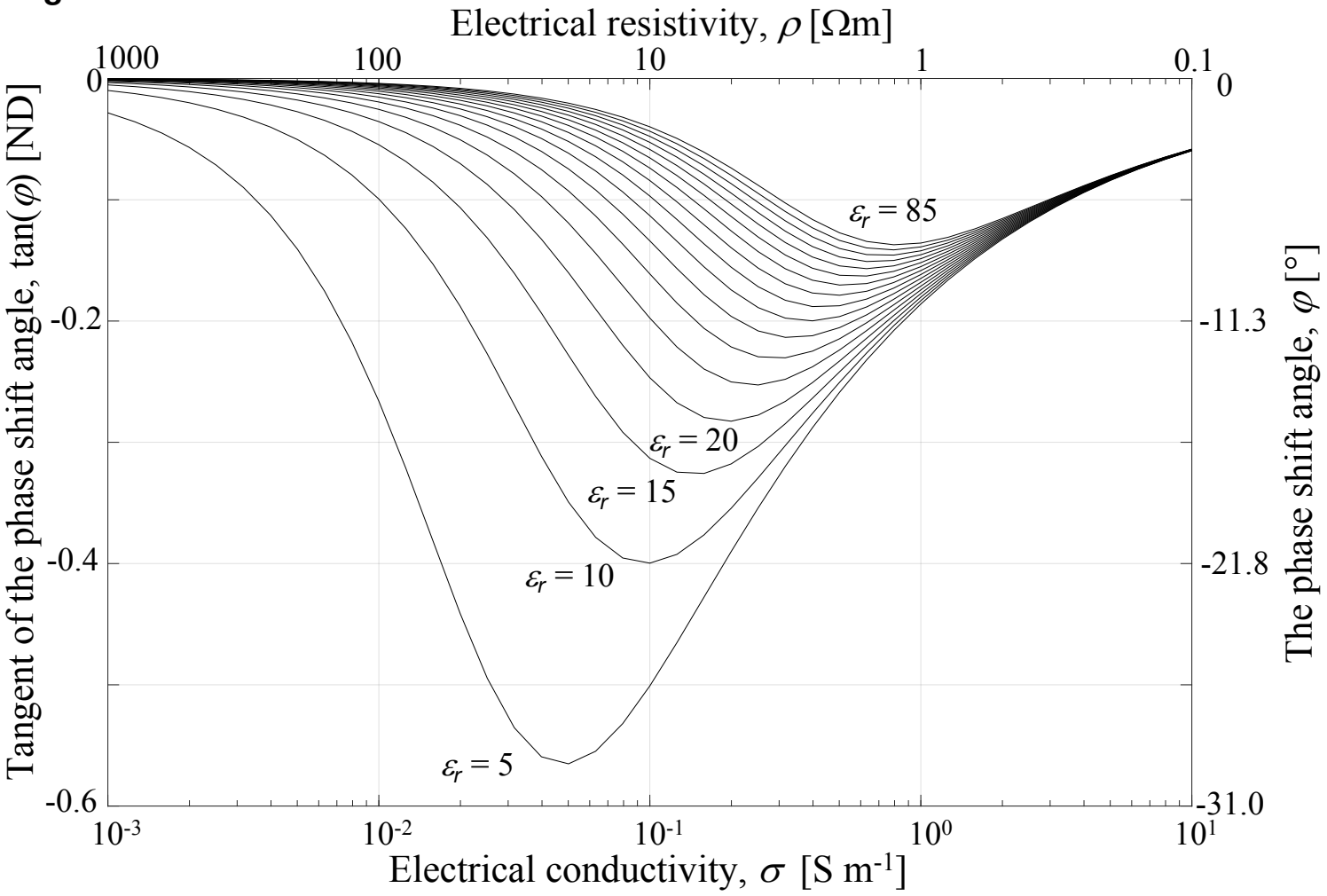

https://doi.org/10.5194/tc-2020-9
Preprint. Discussion started: 6 February 2020
© Author(s) 2020. CC BY 4.0 License.

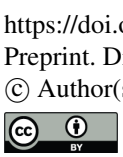

The Cryosphere
Discussions
Open Access
EGU
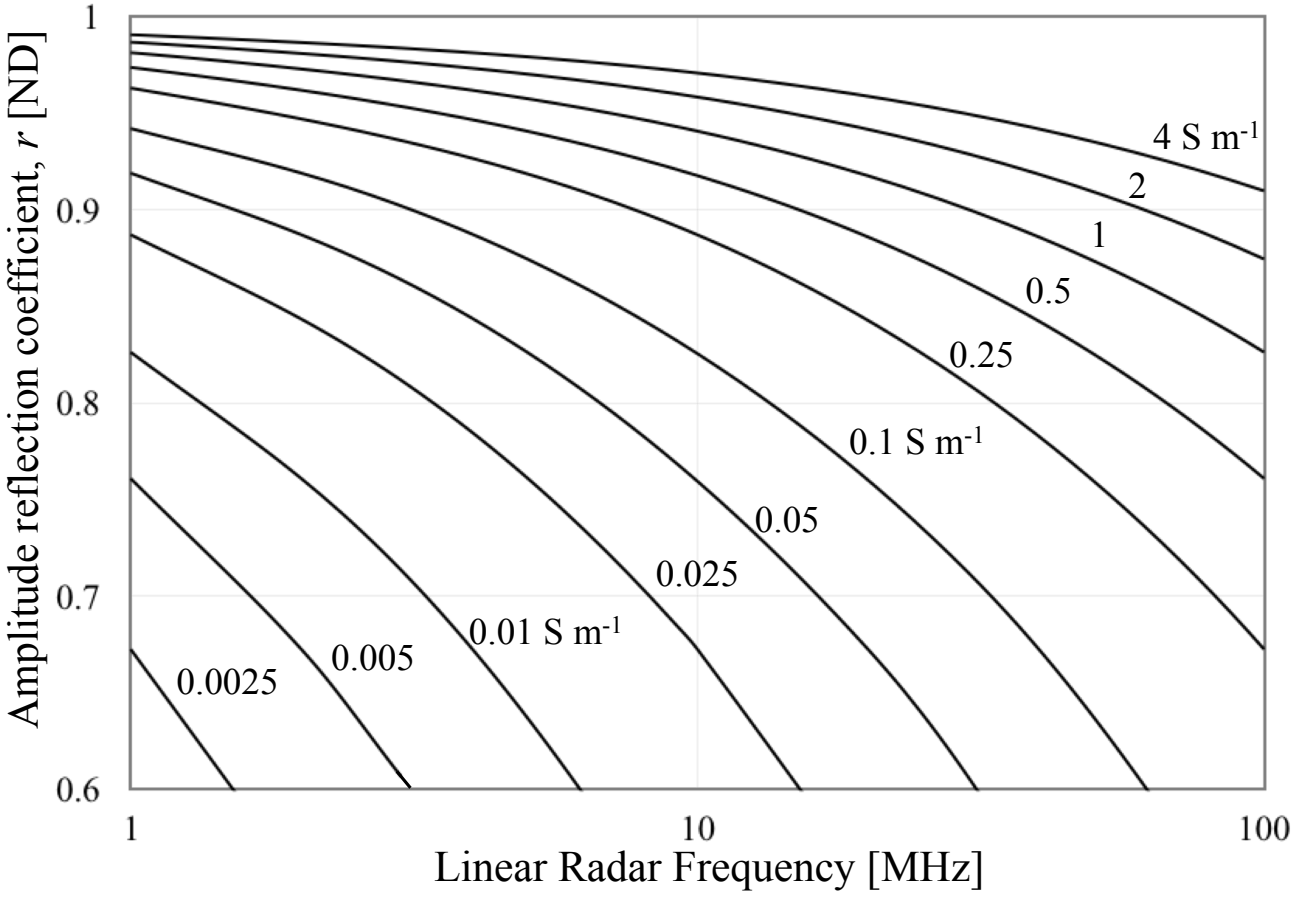
Figure 6